




Article

Structural Variations in Manganese Halide Chain Compounds Mediated by Methylimidazolium Isomers

Ceng Han, David B. Cordes , Alexandra M. Z. Slawin  and Philip Lightfoot * 

School of Chemistry and EaStChem, University of St Andrews, St Andrews KY16 9ST, UK; ch292@st-andrews.ac.uk (C.H.); dbc21@st-andrews.ac.uk (D.B.C.); amzs@st-andrews.ac.uk (A.M.Z.S.)

* Correspondence: pl@st-andrews.ac.uk; Tel.: +44-1334-463841

Received: 25 September 2020; Accepted: 10 October 2020; Published: 13 October 2020



Abstract: The structures of two new hybrid organic–inorganic manganese halide compounds $[1\text{MiH}]\text{MnCl}_3(\text{H}_2\text{O})$ and $[4\text{MiH}]\text{MnCl}_3(\text{H}_2\text{O})$ ($[1\text{MiH}] = 1\text{-methylimidazolium}$, $[4\text{MiH}] = 4\text{-methylimidazolium}$) have been determined by single crystal X-ray diffraction. Both are composed of one dimensional $[\text{MnCl}_3(\text{H}_2\text{O})]_n^-$ edge-sharing octahedral chains. The structures are compared to the previously reported isomeric analogue $[2\text{MiH}]\text{MnCl}_3(\text{H}_2\text{O})$ ($[2\text{MiH}] = 2\text{-methylimidazolium}$), and three closely related compounds. The variations in packing of the inorganic chains are shown to be influenced by hydrogen bonding abilities of the imidazolium or related moieties. Both new compounds show intense red luminescence at ambient temperature under UV irradiation.

Keywords: crystal structure; manganese halides; one dimensional; red luminescence

1. Introduction

The past decade has witnessed much progress in the exploratory study of hybrid inorganic–organic compounds, many of which are related to the perovskite family [1,2]. Such compounds are of interest due to their versatile chemical and physical properties, such as photoluminescence, electronic and photophysical properties [3–5]. In particular, hybrid manganese halide perovskite-related materials have been developed [6,7] because they show significant magnetic, ferroelectric or luminescent properties [8–10]. Conventional perovskites have a general formula ABX_3 and the first classical perovskite, CaTiO_3 consists of a unique framework of corner-sharing TiO_6 octahedra with interstitial Ca^{2+} cations [11]. There are many types of perovskite-related materials, for example two-dimensional layered perovskites, which can be regarded as being derived from ‘slicing’ the perovskite ABX_3 through vertices of the BX_6 octahedra and inserting additional species between these layers [12,13]. Examples amongst manganese halides are $(\text{CH}_3\text{NH}_3)_2\text{MnCl}_4$ [14] and $(\text{NH}_3\text{CH}_2\text{CH}_2\text{NH}_3)\text{MnCl}_4$ [15]. Recently, our group has reported the first layered fluoroperovskite compound, $(en\text{H}_2)\text{MnF}_4$ (en = ethylenediamine ($\text{C}_2\text{H}_8\text{N}_2$)) [16], containing an interlayer organic cation.

Up to now, Xiong’s group reported a series of one-dimensional (1D) organic–inorganic hybrid Mn^{2+} hexagonal perovskite compounds, where the cations occupy the free cavities enclosed by the face-sharing octahedral chains. These compounds exhibit interesting phase transitions, for example, (pyrrolidinium) MnCl_3 [17] and (R)- and (S)-3-(fluoropyrrolidinium) MnCl_3 [18], which have ferroelectric and fluorescence properties. Interestingly, (2-methylimidazolium) $\text{MnCl}_3(\text{H}_2\text{O})$ ($[2\text{MiH}]\text{MnCl}_3(\text{H}_2\text{O})$) [19,20] (2-aminopyridinium) $\text{MnCl}_3(\text{H}_2\text{O})$ [21], (pyrazolium) $\text{MnCl}_3(\text{H}_2\text{O})$ [22], and (pyridinium) $\text{MnCl}_3(\text{H}_2\text{O})$ [23] also adopt a 1D chain structure type, but the octahedra are edge-sharing and, consequently, the structure cannot be regarded as perovskite-like. According to these studies, the luminescence of manganese (II) halide hybrids can be assigned to the $^4\text{T}_{1g}(\text{G}) \rightarrow$

${}^6A_{1g}(S)$ electronic transition of Mn^{2+} . Both edge-sharing and face-sharing octahedral Mn^{2+} ions tend to emit red luminescence [17,18,20,23], whereas, the corner-sharing octahedral Mn^{2+} ions tend to a somewhat higher energy orange emission (581 nm) [10]. However, if a Mn atom is surrounded by four ligands to form an independent MnX_4^{2-} tetrahedral unit, then the weak field strength of tetrahedral coordinated Mn^{2+} exhibits typically green emission (≈ 520 nm) [24,25]. The different interactions of the Mn^{2+} ions can affect luminescence and leads to the 1D organic–inorganic hybrid Mn^{2+} compounds having potential applications not only in optical devices but also in luminescent thermometers and resistance sensors, and so on [17,18,26].

As part of our exploratory search for novel perovskite-related hybrids we have discovered several new compounds which adopt chain structures, structurally unrelated to perovskite, but with similar ABX_3 -type compositions [27,28]. Compared with the various studies of manganese halide materials based on the hexagonal perovskite and layered perovskite structures, the present work focusses on the much less common 1D edge-sharing octahedral chain structure type. Here, we present two new 1D edge-sharing octahedral chain structure compounds, $[1MiH]MnCl_3(H_2O)$ and $[4MiH]MnCl_3(H_2O)$ ($[1MiH]$ = 1-methylimidazolium, $[4MiH]$ = 4-methylimidazolium).

2. Experimental Section

2.1. Chemicals

Manganese chloride tetrahydrate ($MnCl_2 \cdot 4H_2O$, 98%), hydrochloric acid (HCl, 36%, w/w aqueous solution), ethanol absolute (C_2H_5OH , 99.99%), 1-methylimidazole ($C_4N_2H_6$, 99%), and 4-methylimidazole ($C_4N_2H_6$, 98%) were purchased from Alfa Aesar, Lancashire, UK. All chemicals were directly used without further purification.

2.2. Synthesis

For $[1MiH]MnCl_3(H_2O)$, ($C_4N_2H_7MnCl_3(H_2O)$), 1-methylimidazole (246.3 mg, 3 mmol) and manganese chloride tetrahydrate ($MnCl_2 \cdot 4H_2O$) (197.9 mg, 1 mmol) were dissolved in concentrated HCl (1 mL) and ethanol (1 mL). With slow evaporation of the solution, pale pink prismatic crystals were obtained after several days. The powder X-ray diffraction is given in Figure S1.

For $[4MiH]MnCl_3(H_2O)$, ($C_4N_2H_7MnCl_3(H_2O)$), 4-methylimidazole (164.2 mg, 2 mmol) and manganese chloride tetrahydrate ($MnCl_2 \cdot 4H_2O$) (197.9 mg, 1 mmol) were dissolved in concentrated HCl (1 mL) and ethanol (1 mL). With slow evaporation of the solution, pale pink block-shaped crystals were obtained after 1 week. The powder X-ray diffraction is given in Figure S2.

2.3. Characterisation

Single crystal X-ray diffraction data were collected at 173 and 298 K on a Rigaku SCXMini diffractometer using Mo- $K\alpha$ radiation. The same $[1MiH]MnCl_3(H_2O)$ crystal was run at both 173 and 298 K. The $[4MiH]MnCl_3(H_2O)$ crystal used for the 173 K structure was found to be twinned, but the

data were processed to account for the twin law $\begin{pmatrix} -1 & 0 & -0.209 \\ 0.001 & -1.001 & 0 \\ 0 & 0 & 1 \end{pmatrix}$. The refined twin fraction

was 0.21 (2). The $[4MiH]MnCl_3(H_2O)$ crystal used for the 298 K structure achieved good refinements. The data were collected using Rigaku CrystalClear software [29]. Data processed (including correction for Lorentz, polarisation and absorption) using either CrystalClear or CrysAlisPro [30]. Structures were solved by dual-space methods using SHELXT [31] and refined by full-matrix least-squares on F^2 using SHELXL-2018/3 [32] incorporated in the WINGX package [33]. All the hydrogen atoms were treated as riding atoms and all non-H atoms were refined anisotropically. CrystalMaker [34] was used in preparing Figures 1–3.

Crystalline powders of the two samples were measured on a PANalytical EMPYREAN X-ray diffractometer using Cu $K_{\alpha 1}$ ($\lambda = 1.5406$ Å) radiation in the range of 3–70°. Excitation and steady-state

emission spectra were recorded at 298 K using an Edinburgh Instruments F980 fluorimeter. All the samples for the steady-state measurements were excited at 352 nm using a Xenon lamp.

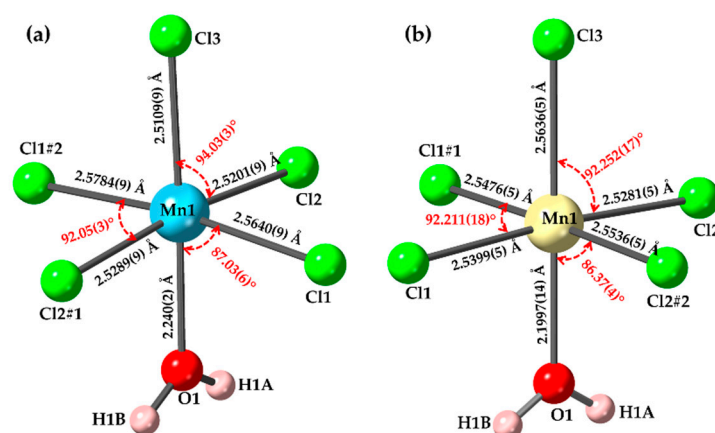


Figure 1. The nature of the distortions within the $[\text{MnCl}_3(\text{H}_2\text{O})]$ chains in (a) $[\text{1MiH}]\text{MnCl}_3(\text{H}_2\text{O})$ and (b) $[\text{4MiH}]\text{MnCl}_3(\text{H}_2\text{O})$ at 173 K. In each case, Cl(3) is a terminal ligand, and the other Cl ligands are bridging, along the chain direction. Symmetry transformations used to generate equivalent atoms: #1 $-x-1, y+1/2, -z-3/2$; #2 $-x-1, y-1/2, -z-3/2$ ($[\text{1MiH}]\text{MnCl}_3(\text{H}_2\text{O})$). #1 $x, -y+1/2, z+1/2$; #2 $x, -y+1/2, z-1/2$ ($[\text{4MiH}]\text{MnCl}_3(\text{H}_2\text{O})$).

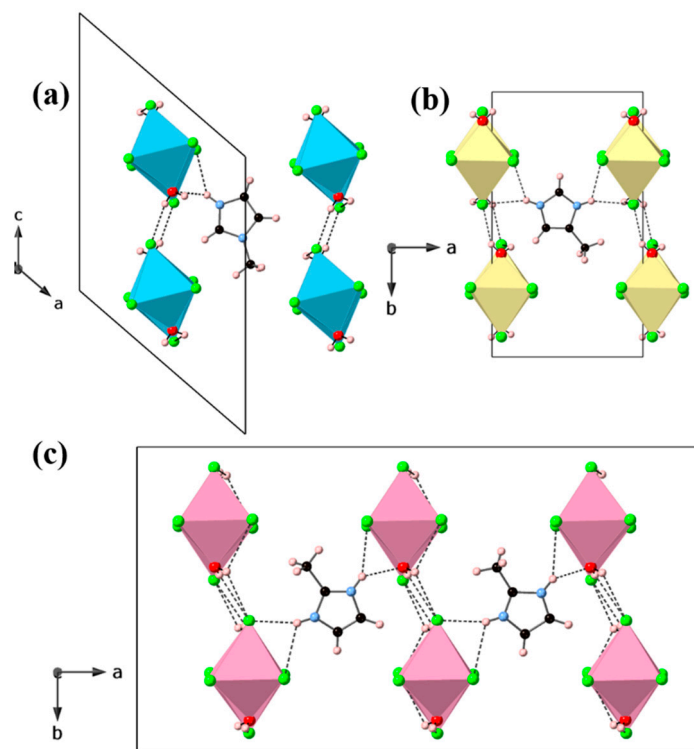


Figure 2. Unit cell packing and hydrogen bonding interactions along the chain direction for (a) $[\text{1MiH}]\text{MnCl}_3(\text{H}_2\text{O})$ along the b -axis, (b) $[\text{4MiH}]\text{MnCl}_3(\text{H}_2\text{O})$ along the c -axis and (c) $[\text{2MiH}]\text{MnCl}_3(\text{H}_2\text{O})$ along the c -axis at 173 K [20].

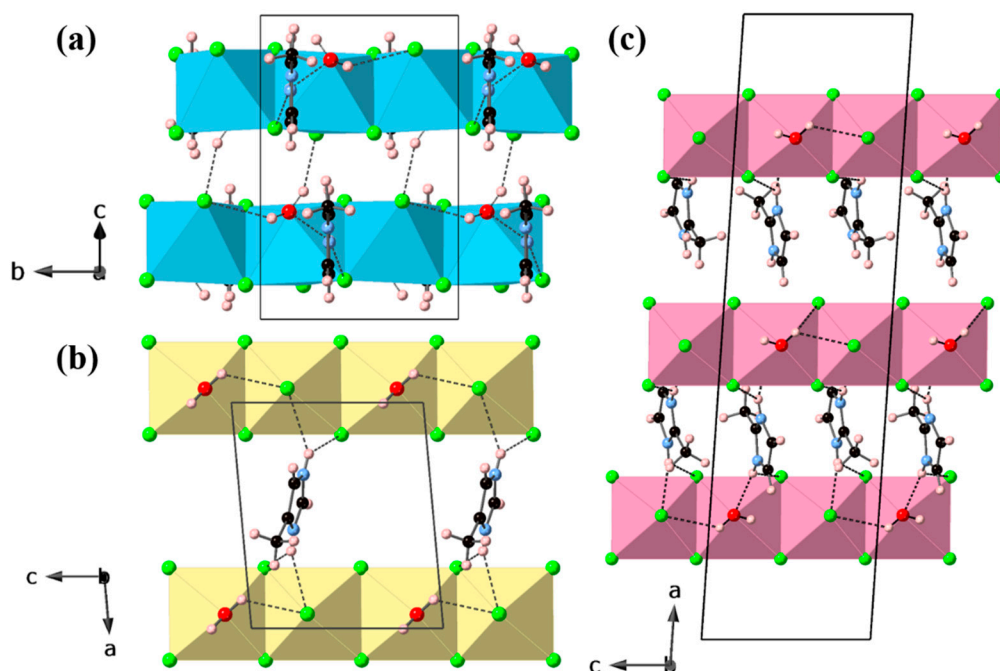


Figure 3. Unit cell packing and hydrogen bonding interactions perpendicular to the chain direction for (a) [1MiH]MnCl₃(H₂O) along the *a*-axis, (b) [4MiH]MnCl₃(H₂O) along the *b*-axis and (c) [2MiH]MnCl₃(H₂O) along the *b*-axis at 173 K [20].

3. Results and Discussion

The single-crystal X-ray structures suggest no phase transitions in the regime $173 < T < 298$ K, with only slight changes in molecular geometry between the two temperatures, so the crystallographic details for the two new compounds will be discussed based on the structures at 173 K. Crystallographic details of the structures at 298 K are provided in the Supplementary Materials. Crystallographic parameters for the two compounds at 173 K are given in Table 1. Both structures are composed of one dimensional [MnCl₃(H₂O)]_{*n*}[−] edge-sharing octahedral chains, separated by the imidazolium moieties. In each case there is one crystallographically unique Mn site and one imidazolium moiety. The significant distortions of the MnCl₃(H₂O) octahedra are shown in Figure 1. For [1MiH]MnCl₃(H₂O) and [4MiH]MnCl₃(H₂O), respectively, the Mn–Cl bond lengths are in the ranges of 2.5109(9)–2.5784(9) and 2.5278(5)–2.5633(5) Å, the Mn–O bond lengths are 2.240(2) and 2.1993(12) Å. The Cl–Mn–Cl bond angles are in the ranges of 87.41(3)–94.46(3) and 87.319(15)–92.635(16)°, the O–Mn–Cl bond angles are in the ranges of 85.64(6)–87.03(6) and 85.58(4)–91.72(4)°, the Mn–Cl–Mn bond angles are in the ranges of 90.73(2)–92.90(2) and 92.032(16)–92.145(16)° at 173 K.

The same type of [MnCl₃(H₂O)]_{*n*}[−] edge-sharing octahedral chain is also seen in the related structure containing an isomeric cation, [2MiH]MnCl₃(H₂O). Moreover, that analogue also crystallises in space group *P*2₁/*c*, and has unit cell metrics at 293 K, *a* = 8.9890(18) Å, *b* = 14.612(3) Å, *c* = 7.2748(15) Å, β = 93.86(3)°, which are clearly similar to those of [4MiH]MnCl₃(H₂O) at 173 K (Table 1). However, in the case of [2MiH]MnCl₃(H₂O) the crystal structure was determined at both 293 and 173 K, and found to display a structural phase transition of order–disorder type around 220 K; ordering of the imidazolium moieties at low temperature leads to a tripling of the *a*-axis. In each of the present cases there is no unit cell tripling at 173 K. Given that each of the three members of this methylimidazolium-based family is based on the same type of inorganic chain, it is of interest to compare both the intra-chain distortions and the nature of the crystal packing of these chains, which is evidently mediated by the shape and hydrogen bonding propensities of the different imidazolium isomers. A comparison of the intra-chain distortions is provided in Table 2. We also include here the three further analogues, which contain the same type of [MnCl₃(H₂O)]_{*n*}[−] chain, but different cyclic amines; these are discussed briefly at the end

of this section. Each of the structures show a similar level of octahedral distortion, and a significant underbonding of the apical Cl ligand. This is compensated in each case by strong H-bonding from the water ligand of a neighbouring chain to the apical Cl (Table 3).

First, comparing the three methylimidazolium compounds, each structure has one unit cell axis of ≈ 7.3 Å, which describes the chain repeat distance of two edge-shared octahedra. The other unit cell metrics differ significantly between the [1MiH] and [2MiH]/[4MiH] compounds reflecting the different packing of inorganic chains between the two unit cell types. Packing of each structure along the chain direction, and perpendicular to this, is shown in Figures 2 and 3. It can be seen from Figures 2 and 3 that in the case of the [1MiH] compound there is no opportunity for inter-chain H-bonding mediated by the imidazole moiety; the single available N-H donor only forms a single N-H—Cl and N-H—O interaction to one neighbouring chain. In contrast, both [2MiH] and [4MiH] analogues do take the opportunity to pack in a similar fashion, due to the availability of additional N-H—Cl interactions to bridge neighbouring chains. The packing of neighbouring chains along the *c*-axis in the latter two compounds (Figure 2) therefore occurs in a ‘parallel’ arrangement, whereas the corresponding chains in [1MiH] exhibit a ‘tilt’ around the chain direction (*b*-axis) relative to each other.

As mentioned above, there are three further closely related compounds reported, which contain the same inorganic chains but different cyclic amine cations, *viz.*, (2-aminopyridinium) $\text{MnCl}_3(\text{H}_2\text{O})$ [21], (pyrazolium) $\text{MnCl}_3(\text{H}_2\text{O})$ [22] and (pyridinium) $\text{MnCl}_3(\text{H}_2\text{O})$ [23]. Again, each of these crystal structures has a unit cell axis of ≈ 7.3 Å, describing the chain repeat distance of two edge-shared octahedra. The details of the unit cell metrics, crystal symmetry, and comparative crystal structure plots for these three analogues are given in Table S1 and Figure S3. Interestingly, the pyridinium analogue has essentially the same structural architecture as the [1MiH] compound introduced here: there is hydrogen bonding to only one inorganic chain. The pyrazolium and 2-aminopyridinium analogues have enhanced H-bonding opportunities, which lead to expanded unit cells (effectively doubled unit cell volumes) caused by ‘out-of-phase’ tilting of adjacent octahedral chains along the chain axis.

Table 1. Crystal structure data for [1MiH] $\text{MnCl}_3(\text{H}_2\text{O})$ and [4MiH] $\text{MnCl}_3(\text{H}_2\text{O})$ at 173 K.

Compound	[1MiH] $\text{MnCl}_3(\text{H}_2\text{O})$	[4MiH] $\text{MnCl}_3(\text{H}_2\text{O})$
Formula	$\text{C}_4\text{N}_2\text{H}_7\text{MnCl}_3(\text{H}_2\text{O})$	$\text{C}_4\text{N}_2\text{H}_7\text{MnCl}_3(\text{H}_2\text{O})$
Formula weight	262.42	262.42
Crystal system	Monoclinic	Monoclinic
Space group	$P2_1/c$	$P2_1/c$
<i>a</i> /Å	11.6861 (6)	8.6344 (6)
<i>b</i> /Å	7.2891 (4)	15.1238 (6)
<i>c</i> /Å	14.7870 (9)	7.3164 (3)
β /°	130.932 (3)	95.069(5)
<i>V</i> /Å ³	951.59 (10)	951.68 (9)
<i>Z</i>	4	4
Measured ref	11543	9328
Independent ref	3115	2565
	[R(int) = 0.053]	[R(int) = 0.0315]
GOOF	1.059	1.028
Final R indices (<i>I</i> > 2σ(<i>I</i>))	$R_1 = 0.0513$ $wR_2 = 0.0953$	$R_1 = 0.0318$ $wR_2 = 0.0651$

Table 2. Calculated bond length distortions, bond angle variance and bond valence sums for [1MiH]MnCl₃(H₂O) and [4MiH]MnCl₃(H₂O) at 173 K, and previously reported [2MiH]MnCl₃(H₂O) (173 K) [20], (2-aminopyridinium)MnCl₃(H₂O) (298 K) [21], (pyrazolium)MnCl₃(H₂O) (100 K) [22] and (pyridinium)MnCl₃(H₂O) (153 K) [23].

Compound	$\Delta d (\times 10^4)$	σ^2	$\sum v$ (Mn)	$\sum v$ (Cl1)	$\sum v$ (Cl2)	$\sum v$ (Cl3)	$\sum v$ (O1)
[1MiH]MnCl ₃ (H ₂ O)	20.92	12.24	1.93	0.61	0.69	0.36	0.27
[4MiH]MnCl ₃ (H ₂ O)	27.15	6.52	1.93	0.66	0.66	0.31	0.30
[2MiH]MnCl ₃ (H ₂ O)	21.46	16.53	1.98	0.61	0.74	0.36	0.27
(2-aminopyridinium)MnCl ₃ (H ₂ O)	33.85	9.22	1.93	0.64	0.60	0.36	0.32
(pyrazolium)MnCl ₃ (H ₂ O)	24.72	7.22	1.99	0.72	0.63	0.34	0.29
(pyridinium)MnCl ₃ (H ₂ O)	22.77	10.69	1.95	0.60	0.70	0.37	0.27

Note: The bond length distortion was calculated using equation $\Delta d = \left(\frac{1}{6}\right) \sum \left[\frac{d_n - d}{d}\right]^2$ [35], where d is the average Mn-Cl and Mn-O bond distance and d_n are the six individual bond distances. The bond angle variance of each octahedron from the ideal 90° of an undistorted structure was calculated using equation $\sigma^2 = \sum_{i=1}^{12} \frac{(\sigma_i - 90)^2}{11}$ [36], where σ_i is the individual Cl-Mn-Cl and O-Mn-Cl angle. The bond valence was calculated using equation $v_{ij} = \exp\left(\frac{R_0 - d}{b}\right)$ [37], where d is the individual bond length, R_0 is a constant for a particular bond type, here $R_0 = 2.133$ Å for the Mn-Cl bond and $R_0 = 1.753$ Å for the Mn-O bond, and $b = 0.37$ Å, a universal constant. The bond valence sum $\sum v_i$ is the summation of the individual bond valences.

Table 3. Hydrogen bonds for [1MiH]MnCl₃(H₂O) and [4MiH]MnCl₃(H₂O) at 173 K, and previously reported [2MiH]MnCl₃(H₂O) at 173 K (Å and °) [20].

Compound	D-H ... A	d(D-H)	d(H ... A)	d(D ... A)	∠(DHA)
[1MiH]MnCl ₃ (H ₂ O)	N2-H2 ... Cl1#1	0.88	2.54	3.256(3)	139.1
	N2-H2 ... O1	0.88	2.38	3.018(4)	129.9
	O1-H1B ... Cl3#2	0.95	2.56	3.171(2)	122.6
	O1-H1A ... Cl3#3	0.95	2.32	3.201(2)	154.0
[4MiH]MnCl ₃ (H ₂ O)	O1-H1A ... Cl3#3	0.95	2.41	3.227(2)	144.0
	O1-H1B ... Cl3#2	0.95	2.54	3.177(2)	124.2
	N1-H1 ... Cl1#1	0.88	2.82	3.363(2)	121.8
	N1-H1 ... Cl3	0.88	2.47	3.263(2)	149.9
	N2-H2 ... Cl2#4	0.88	2.65	3.279(2)	129.1
	N2-H2 ... Cl3#5	0.88	2.63	3.349(2)	140.0
[2MiH]MnCl ₃ (H ₂ O)	N1-H1B...O2	0.88	2.25	2.959(11)	138
	N1-H1B...Cl5	0.88	2.66	3.362(9)	137
	N2-H2B...Cl8	0.88	2.30	3.125(9)	157
	N2-H2B...Cl9	0.88	2.98	3.496(8)	119
	N3-H3A...O3#7	0.88	2.25	2.831(10)	137
	N3-H3A...Cl9#7	0.88	2.80	3.417(8)	143
	N4-H4D...Cl4	0.88	2.36	3.168(8)	154
	N4-H4D...Cl5	0.88	2.99	3.518(9)	120
	O1—H1C...Cl1#1	0.85	2.67	3.180(6)	128
	O1—H1D...Cl8	0.85	2.70	3.152(6)	122
	O2—H2C...Cl4#1	0.85	2.60	3.174(7)	126
	O2—H2D...Cl4#5	0.85	2.59	3.143(6)	124
	O3—H3B...Cl8#2	0.85	2.64	3.160(7)	129
	O3—H3C...Cl1#6	0.85	2.73	3.185(6)	122

Note: Symmetry transformations used to generate equivalent atoms: #1 $-x-1, y-1/2, -z-3/2$; #2 $-x-1, y+1/2, -z-3/2$; #3 $x, -y+1/2, z-1/2$ ([1MiH]MnCl₃(H₂O)). #1 $x, -y+1/2, z+1/2$; #2 $x, -y+1/2, z-1/2$; #4 $x-1, -y+1/2, z-1/2$; #5 $x-1, y, z$ ([4MiH]MnCl₃(H₂O)). #7 $x, y-1, z$; #1 $x, -y+1/2, z-1/2$; #5 $-x+1, y+1/2, -z+1/2$; #2 $x, -y+3/2, z+1/2$; #6 $x, y+1, z$; ([2MiH]MnCl₃(H₂O)).

A previous study of the [2MiH] compound [20] highlighted an unusual property of a reversible optoelectronic phase transition, accompanied by both dielectric and photoluminescent switching effects. Although the present compounds do not display any structural phase transitions in the temperature regime studied here, both compounds do show intense red luminescence at ambient temperature under UV irradiation, similar to that observed in (CH₆N₃)₂MnCl₄ [38] and (CH₃)₄NMnCl₃ [39]. Both of those compounds feature face-sharing, rather than edge-sharing, units of MnCl₆ octahedra. The excitation and emission spectra of the two compounds were investigated (Figure 4). As can be seen, both

compounds display similar excitation spectra monitored at 620 nm. All the excitation spectra of the two compounds contain six sharp peaks, at around 527, 447, 418, 367, 352, 331 nm, and are comparable to the excitation spectra of $[2\text{MiH}]\text{MnCl}_3(\text{H}_2\text{O})$ [20], in which the most intense band at 352 nm serves as an excitation wavelength. Emission spectra were recorded at this excitation wavelength. The emission spectra revealed that all two compounds featured similar peaks at 630 and 632 nm for $[1\text{MiH}]\text{MnCl}_3(\text{H}_2\text{O})$ and $[4\text{MiH}]\text{MnCl}_3(\text{H}_2\text{O})$, respectively. Such interesting red luminescence is produced by the ${}^4\text{T}_{1\text{g}}(\text{G}) \rightarrow {}^6\text{A}_{1\text{g}}(\text{S})$ transition (i.e., $(t_{2\text{g}})^3(e_{\text{g}})^2 \rightarrow (t_{2\text{g}})^4(e_{\text{g}})^1$ electronic transition [17,40]) and similar emission energies have been reported in complexes of octahedrally coordinated Mn^{2+} ions in both edge-sharing and face-sharing environments [41]. In the case of corner-sharing octahedral Mn^{2+} ions, this tends to a somewhat higher energy orange emission (581 nm) [10], while those compounds with Mn^{2+} ions in the tetrahedral environment usually display green emissions (≈ 520 nm) [42–44].

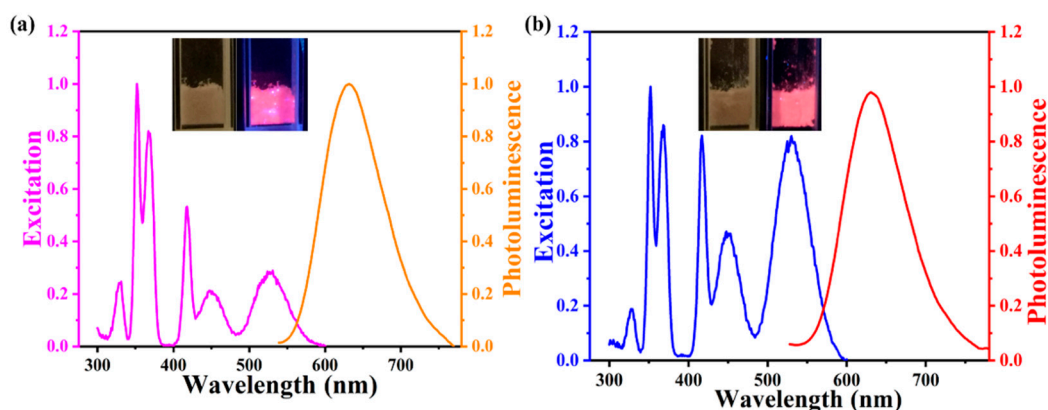


Figure 4. The excitation and emission spectra at room temperature of (a) $[1\text{MiH}]\text{MnCl}_3(\text{H}_2\text{O})$, and (b) $[4\text{MiH}]\text{MnCl}_3(\text{H}_2\text{O})$. The insets of both (a,b) show pale pink crystals under ambient light and a bright pink glow under UV.

4. Conclusions

In conclusion, we prepared two new compounds composed of one dimensional $[\text{MnCl}_3(\text{H}_2\text{O})]_n^-$ edge-sharing octahedral chains. Each of the structures was discussed in detail in terms of octahedral distortions, crystal packing and H-bonding environments. These new examples were also compared, structurally, to the previously reported analogue $[2\text{MiH}]\text{MnCl}_3(\text{H}_2\text{O})$ and three further related compounds containing the same type of inorganic chain but different molecular cations. It can be seen that subtle changes in H-bonding opportunities, caused by key changes in the chemical nature of the molecular cations, leads to variations in the nature of packing of the inorganic chains. The preliminary photophysical properties were studied by their excitation and emission spectra: both new compounds exhibit intense red luminescence under a UV excitation. Further studies of related compounds are therefore merited in order to ascertain more specific structural details that may govern their luminescence properties and may also be exploited for triggering phase transitions, and consequent switchable physical properties, in this family of materials.

Supplementary Materials: The following are available online at <http://www.mdpi.com/2073-4352/10/10/930/s1>, Figure S1. Raw and calculated PXRD data for $[1\text{MiH}]\text{MnCl}_3(\text{H}_2\text{O})$ at room temperature; Figure S2. Raw and calculated PXRD data for $[4\text{MiH}]\text{MnCl}_3(\text{H}_2\text{O})$ at room temperature Figure S3. Unit cell packing and hydrogen bonding interactions along the chain direction for (a) (2-aminopyridinium) $\text{MnCl}_3(\text{H}_2\text{O})$ (298 K) along the *c*-axis, (b) (pyrazolium) $\text{MnCl}_3(\text{H}_2\text{O})$ (100 K) along the *a*-axis and (c) (pyridinium) $\text{MnCl}_3(\text{H}_2\text{O})$ (153 K) along the *b*-axis; Table S1. Unit cell parameters for (2-aminopyridinium) $\text{MnCl}_3(\text{H}_2\text{O})$ (298 K), (pyrazolium) $\text{MnCl}_3(\text{H}_2\text{O})$ (100 K) and (pyridinium) $\text{MnCl}_3(\text{H}_2\text{O})$ (153 K); Table S2: Crystallographic data for the two compounds at 298 K; Table S3: Hydrogen bonds for the two compounds at 298 K; Table S4. Selected bond lengths (Å) and bond angles (°) versus temperature for $[1\text{MiH}]\text{MnCl}_3(\text{H}_2\text{O})$; Table S5: Selected bond lengths (Å) and bond angles (°) versus temperature for $[4\text{MiH}]\text{MnCl}_3(\text{H}_2\text{O})$.

Author Contributions: C.H. carried out all the synthesis and further characterisation, and some of the single-crystal X-ray diffraction crystallography. D.B.C. and A.M.Z.S. assisted with some of the single crystal X-ray data collection. P.L. coordinated the project and writing of the paper, with the approval of all authors. All authors have read and agreed to the published version of the manuscript.

Funding: This research was funded by the University of St Andrews and the China Scholarship Council (studentship to CH), grant number “201806050003”.

Conflicts of Interest: The authors declare no conflict of interest.

References

- Protesescu, L.; Yakunin, S.; Bodnarchuk, M.I.; Krieg, F.; Caputo, R.; Hendon, C.H.; Yang, R.X.; Walsh, A.; Kovalenko, M.V. Nanocrystals of cesium lead halide perovskites (CsPbX_3 , $X = \text{Cl, Br, and I}$): Novel optoelectronic materials showing bright emission with wide color gamut. *Nano Lett.* **2015**, *15*, 3692–3696. [[CrossRef](#)] [[PubMed](#)]
- Wang, C.L.; Song, Z.N.; Li, C.W.; Zhao, D.W.; Yan, Y.F. Low-Bandgap mixed Tin-Lead perovskites and their applications in all-perovskite tandem solar cells. *Adv. Funct. Mater.* **2019**, *29*, 1808801. [[CrossRef](#)]
- Mao, L.; Ke, W.; Pedesseau, L.; Wu, Y.; Katan, C.; Even, J.; Wasielewski, M.R.; Stoumpos, C.C.; Kanatzidis, M.G. Hybrid Dion–Jacobson 2D lead iodide perovskites. *J. Am. Chem. Soc.* **2018**, *140*, 3775–3783. [[CrossRef](#)] [[PubMed](#)]
- Stoumpos, C.C.; Cao, D.H.; Clark, D.J.; Young, J.; Rondinelli, J.M.; Jang, J.I.; Hupp, J.T.; Kanatzidis, M.G. Ruddlesden–Popper hybrid lead iodide perovskite 2D homologous semiconductors. *Chem. Mater.* **2016**, *28*, 2852–2867. [[CrossRef](#)]
- Jacobsson, T.J.; Schwan, L.J.; Ottosson, M.; Hagfeld, A.; Edvinsson, T. Determination of thermal expansion coefficients and locating the temperature-induced phase transition in methylammonium lead perovskites using x-ray diffraction. *Inorg. Chem.* **2015**, *54*, 10678–10685. [[CrossRef](#)] [[PubMed](#)]
- Sourisseau, C.; Lucazeau, G. Vibrational study of phase transitions in $(\text{NH}_3(\text{CH}_2)_3\text{NH}_3)\text{MnCl}_4$. *J. Raman Spectrosc.* **1979**, *8*, 311–319. [[CrossRef](#)]
- Park, S.H.; Oh, I.H.; Park, S.; Park, Y.B.; Kim, J.H.; Huh, Y.D. Canted antiferromagnetism and spin reorientation transition in layered inorganic–organic perovskite $(\text{C}_6\text{H}_5\text{CH}_2\text{CH}_2\text{NH}_3)_2\text{MnCl}_4$. *Dalton Trans.* **2012**, *41*, 1237–1242. [[CrossRef](#)] [[PubMed](#)]
- Kojima, N.; Ban, T.; Tsujikawa, I. Magnon sideband of the $^4\text{T}_{2g}$ (4D) state in the quasi two-dimensional antiferromagnet $(\text{C}_2\text{H}_5\text{NH}_3)_2\text{MnCl}_4$. *J. Phys. Soc.* **1978**, *44*, 923–929. [[CrossRef](#)]
- Ye, H.Y.; Zhou, Q.; Niu, X.; Liao, W.Q.; Fu, D.W.; Zhang, Y.; You, Y.M.; Wang, J.; Chen, Z.N.; Xiong, R.G. High-temperature ferroelectricity and photoluminescence in a hybrid organic–inorganic compound: $(3\text{-Pyrrolinium})\text{MnCl}_3$. *J. Am. Chem. Soc.* **2015**, *137*, 13148–13154. [[CrossRef](#)]
- Lv, X.H.; Liao, W.Q.; Li, P.F.; Mao, C.Y.; Zhang, Y. Dielectric and photoluminescence properties of a layered perovskite-type organic–inorganic hybrid phase transition compound: $\text{NH}_3(\text{CH}_2)_5\text{NH}_3\text{MnCl}_4$. *J. Mater. Chem. C* **2016**, *4*, 1881–1885. [[CrossRef](#)]
- Kay, H.F.; Bailey, P.C. Structure and properties of CaTiO_3 . *Acta Crystallogr.* **1957**, *10*, 219–226. [[CrossRef](#)]
- Saparov, B.; Mitzi, D.B. Organic–inorganic perovskites: Structural versatility for functional materials design. *Chem. Rev.* **2016**, *116*, 4558–4596. [[CrossRef](#)] [[PubMed](#)]
- Yu, Y.; Zhang, D.D.; Yang, P.D. Ruddlesden–Popper phase in two-dimensional inorganic halide perovskites: A plausible model and the supporting observations. *Nano Lett.* **2017**, *17*, 5489–5494. [[CrossRef](#)] [[PubMed](#)]
- Van Amstel, W.D.; De Jongh, L.J. Magnetic measurements on $(\text{CH}_3\text{NH}_3)_2\text{MnCl}_4$, a quasi two-dimensional Heisenberg antiferromagnet. *Solid State Commun.* **1972**, *11*, 1423–1429. [[CrossRef](#)]
- Arend, H.; Tichy, K.; Baberschke, K.; Rys, F. Chloride perovskite layer compounds of $[\text{NH}_3(\text{CH}_2)_n\text{NH}_3]\text{MnCl}_4$ formula. *Solid State Commun.* **1976**, *18*, 999–1003. [[CrossRef](#)]
- Li, T.; Clulow, R.; Bradford, A.J.; Lee, S.L.; Slawin, A.M.Z.; Lightfoot, P. A hybrid fluoride layered perovskite, $(\text{enH}_2)\text{MnF}_4$. *Dalton Trans.* **2019**, *48*, 4784–4787. [[CrossRef](#)]
- Zhang, Y.; Liao, W.Q.; Fu, D.W.; Ye, H.Y.; Chen, Z.N.; Xiong, R.G. Highly efficient red-light emission in an organic–inorganic hybrid ferroelectric: $(\text{pyrrolidinium})\text{MnCl}_3$. *J. Am. Chem. Soc.* **2015**, *137*, 4928–4931. [[CrossRef](#)]

18. Ai, Y.; Chen, X.G.; Shi, P.P.; Tang, Y.Y.; Li, P.F.; Liao, W.Q.; Xiong, R.G. Fluorine Substitution Induced High T_c of Enantiomeric Perovskite Ferroelectrics: (R)- and (S)-3-(Fluoropyrrolidinium)MnCl₃. *J. Am. Chem. Soc.* **2019**, *141*, 4474–4479. [\[CrossRef\]](#)
19. Hachula, B.; Pedras, M.; Nowak, M.; Kusz, J.; Pentak, D.; Borek, J. The crystal structure and spectroscopic properties of catena-(2-methylimidazolium bis (μ_2 -chloro)-aqua-chloromanganese (II)). *J. Serbian Chem. Soc.* **2011**, *76*, 235–247. [\[CrossRef\]](#)
20. Guo, Q.; Zhang, W.Y.; Chen, C.; Ye, Q.; Fu, D.W. Red-light emission and dielectric reversible double opto-electronic switches in a hybrid multifunctional material: (2-methylimidazolium)MnCl₃(H₂O). *J. Mater. Chem. C* **2017**, *5*, 5458–5464. [\[CrossRef\]](#)
21. Su, C.W.; Wu, C.P.; Chen, J.D.; Liou, L.S.; Wang, J.C. Synthesis and structural characterization of two chain complexes of Mn (II) containing 2-aminopyridinium. *Inorg. Chem. Commun.* **2002**, *5*, 215–219. [\[CrossRef\]](#)
22. Adams, C.J.; Kurawa, M.A.; Orpen, A.G. Coordination chemistry in the solid state: Reactivity of manganese and cadmium chlorides with imidazole and pyrazole and their hydrochlorides. *Inorg. Chem.* **2010**, *49*, 10475–10485. [\[CrossRef\]](#)
23. Li, C.Y.; Bai, X.W.; Guo, Y.C.; Zou, B.S. Tunable emission properties of manganese chloride small single crystals by pyridine incorporation. *ACS Omega* **2019**, *4*, 8039–8045. [\[CrossRef\]](#) [\[PubMed\]](#)
24. Bai, X.; Zhong, H.Z.; Chen, B.K.; Chen, C.; Han, J.B.; Zeng, R.S.; Zou, B.S. Pyridine-modulated Mn ion emission properties of C₁₀H₁₂N₂MnBr₄ and C₅H₆NMnBr₃ single crystals. *J. Phys. Chem. C* **2018**, *122*, 3130–3137. [\[CrossRef\]](#)
25. Chen, S.Q.; Gao, J.M.; Chang, J.Y.; Zhang, Y.; Feng, L. Organic-inorganic manganese (II) halide hybrids based paper sensor for the fluorometric determination of pesticide ferbam. *Sens. Actuators B Chem.* **2019**, *297*, 126701. [\[CrossRef\]](#)
26. Jiang, C.; Zhong, N.; Luo, C.; Lin, H.; Zhang, Y.; Peng, H.; Duan, C.G. (Diisopropylammonium)₂MnBr₄: A multifunctional ferroelectric with efficient green-emission and excellent gas sensing properties. *Chem. Commun.* **2017**, *53*, 5954–5957. [\[CrossRef\]](#)
27. Guo, Y.Y.; Yang, L.J.; Lightfoot, P. Three new lead iodide chain compounds, APbI₃, templated by molecular cations. *Crystals* **2019**, *9*, 616. [\[CrossRef\]](#)
28. Guo, Y.Y.; Lightfoot, P. Structural diversity of lead halide chain compounds, APbX₃, templated by isomeric molecular cations. *Dalton Trans.* **2020**, *49*, 12767–12775. [\[CrossRef\]](#)
29. Rigaku. *CrystalClear*; Rigaku Corporation: Tokyo, Japan, 2014.
30. Rigaku Oxford Diffraction. *CrysAlisPro v1.171.40.40a*; Rigaku Corporation: Oxford, UK, 2015.
31. Sheldrick, G.M. SHELXT—Integrated space-group and crystal-structure determination. *Acta Crystallogr. Sect. A Found. Crystallogr.* **2015**, *71*, 3–8. [\[CrossRef\]](#)
32. Sheldrick, G.M. Crystal structure refinement with SHELXL. *Acta Crystallogr. Sect. C Struct. Chem.* **2015**, *71*, 3–8. [\[CrossRef\]](#)
33. Farrugia, L.J. WinGX and ORTEP for Windows: An update. *J. Appl. Cryst.* **2012**, *45*, 849–854. [\[CrossRef\]](#)
34. Palmer, D.C. *CrystalMaker*; Agilent Technologies Ltd.: Yarnton, Oxfordshire, UK, 2014.
35. Lufaso, M.W.; Woodward, P.M. Jahn-Teller distortions, cation ordering and octahedral tilting in perovskites. *Acta Crystallogr. Sect. B Struct. Sci.* **2004**, *60*, 10–20. [\[CrossRef\]](#) [\[PubMed\]](#)
36. Robinson, K.; Gibbs, G.V.; Ribbe, P.H. Quadratic Elongation: A Quantitative Measure of Distortion in Coordination Polyhedra. *Science* **1971**, *172*, 567–570. [\[CrossRef\]](#) [\[PubMed\]](#)
37. Brese, N.E.; O'Keeffe, M. Bond-valence parameters for solids. *Acta Cryst. B* **1991**, *47*, 192–197. [\[CrossRef\]](#)
38. Sen, A.; Swain, D.; Row, T.N.G.; Sundaresan, A. Unprecedented 30 K hysteresis across switchable dielectric and magnetic properties in a bright luminescent organic-inorganic halide (CH₆N₃)₂MnCl₄. *J. Mater. Chem. C* **2019**, *7*, 4838–4845. [\[CrossRef\]](#)
39. Nataf, L.; Rodríguez, F.; Valiente, R. Spectroscopic and luminescence properties of (CH₃)₄NMnCl₃: A sensitive Mn²⁺-based pressure gauge. *High Press Res.* **2009**, *29*, 653–659. [\[CrossRef\]](#)
40. Orgel, L.E. Phosphorescence of solids containing the manganous or ferric ions. *J. Chem. Phys.* **1955**, *23*, 1958. [\[CrossRef\]](#)
41. Qin, Y.Y.; She, P.F.; Huang, X.M.; Huang, W.; Zhao, Q. Luminescent manganese (II) complexes: Synthesis, properties and optoelectronic applications. *Coord. Chem. Rev.* **2020**, *416*, 213331. [\[CrossRef\]](#)

42. Barreda-Argueso, J.A.; Nataf, L.; Rodriguez-Lazcano, Y.; Aguado, F.; Gonzalez, J.; Valiente, R.; Rodriguez, F.; Wilhelm, H.; Jephcoat, A.P. Bulk and molecular compressibilities of organic–inorganic hybrids $[(CH_3)_4N]_2MnX_4$ ($X = Cl, Br$); role of intermolecular interactions. *Inorg. Chem.* **2014**, *53*, 10708–10715. [[CrossRef](#)]
43. Chen, J.; Zhang, Q.; Zheng, F.K.; Liu, Z.F.; Wang, S.H.; Wu, A.Q.; Guo, G.C. Intense photo-and tribo-luminescence of three tetrahedral manganese (II) dihalides with chelating bidentate phosphine oxide ligand. *Dalton Trans.* **2015**, *44*, 3289–3294. [[CrossRef](#)]
44. Xu, L.J.; Lin, X.S.; He, Q.Q.; Worku, M.; Ma, B.W. Highly efficient eco-friendly X-ray scintillators based on an organic manganese halide. *Nat. Commun.* **2020**, *11*, 1–7. [[CrossRef](#)] [[PubMed](#)]



© 2020 by the authors. Licensee MDPI, Basel, Switzerland. This article is an open access article distributed under the terms and conditions of the Creative Commons Attribution (CC BY) license (<http://creativecommons.org/licenses/by/4.0/>).